J|A|C|S
ARTICLES

Published on Web 04/20/2009

Unusual Interchromophoric Interactions in β,β′ Directly and Doubly Linked Corrole Dimers: Prohibited Electronic Communication and Abnormal Singlet Ground States

Sung Cho,[†] Jong Min Lim,[†] Satoru Hiroto,[‡] Pyosang Kim,[†] Hiroshi Shinokubo,*[,§] Atsuhiro Osuka,*[,‡] and Dongho Kim*[,†]

Spectroscopy Laboratory for Functional π-Electronic Systems and Department of Chemistry, Yonsei University, Seoul 120-749, Korea, Department of Chemistry, Graduate School of Science, Kyoto University, Kyoto 606-8502, Japan, and Department of Applied Chemistry, Graduate School of Engineering, Nagoya University, Nagoya 464-8603, Japan

Received January 12, 2009; E-mail: hshino@apchem.nagoya-u.ac.jp; osuka@kuchem.kyoto-u.ac.jp; dongho@yonsei.ac.kr

Abstract: Directly and doubly β,β′-linked corrole dimers (**DH$_3$CD**, **DH$_2$CD**, and **DZnCD**) are excellent platforms for the investigation of intercorrole interactions because of their enforced coplanar geometries and short edge-to-edge distances. Through the use of these molecules along with the reference monomer **H$_3$CM** and the singly β,β′-linked corrole dimer **SH$_3$CD**, the intercorrole interactions have been systematically studied by density functional theory calculations, ultrafast photophysical measurements, and two-photon absorption measurements. A particular focus was placed on revealing factors that are important for the induced photophysical properties of the doubly linked corrole dimers compared with corrole monomer. In the doubly linked corrole dimers, strong molecular orbital interactions caused by the coplanar geometry and the short interchromophoric distance give rise to perturbations of the electronic states that are responsible for the red-shifted and intensified Q-like band in **DH$_3$CD** and the broad NIR absorption bands and fast excitation-energy relaxation processes in **DH$_2$CD** and **DZnCD**. On the other hand, electronic communication between corrole units is prohibited by the structurally constrained octagonal core in the center, so each constituent corrole unit in the doubly linked corrole dimers maintains an intrinsic π-conjugation system. Consequently, the overall aromaticity of the directly linked corrole dimers can be explained in terms of a linear sum of two constituent corrole monomers, and the singlet biradical character of **DH$_2$CD** and **DZnCD** can be understood in terms of two unpaired electrons (one from each constituent oxidized corrole monomer) and their appropriate interaction. In addition, the nonlinear optical properties of **DH$_2$CD** and **DZnCD** with singlet biradical character have been confirmed to be significantly enhanced compared with those of closed-shell **DH$_3$CD**. Collectively, double β,β′-linkages of corroles provide the coplanar geometry with a short interchromophoric distance and the strained octagonal core that play key roles in allowing the strong molecular orbital interactions and restricting the electronic communication between the two corroles, respectively.

I. Introduction

Corroles are a class of tetrapyrrolic macrocycles with three meso carbons and one direct pyrrole−pyrrole bond.[1,2] At the same time, the fully conjugated aromatic macrocycles of corroles make them quite close to porphyrins in terms of strong absorption and fluorescence in the visible region, photochemical stability, and tuning of optical and redox properties by appropriate metalation and β- or meso-carbon substitution. On the other hand, the direct pyrrole−pyrrole bond and three inner NH hydrogens induce nonplanar structures with lower symmetry, giving rise to unique characteristics such as chemical instability and high fluorescence quantum yield compared with their porphyrin counterparts.[3,4] Although the first synthesis of corroles was reported in 1964,[1a] the complicated synthetic procedure and low yield have been a great challenge for further investigations. The chemistry of corroles has been activated by the recent development of facile synthetic methods of 5,10,15-triaryl-substituted corroles[5−7] but still remains unexplored in comparison to that of porphyrins. In particular, covalently linked corrole

[†] Yonsei University.
[‡] Kyoto University.
[§] Nagoya University.

(1) (a) Johnson, A. W.; Kay, I. T. *Proc. Chem. Soc., London* **1964**, 89. (b) Johnson, A. W. *Pure Appl. Chem.* **1970**, *23*, 375.
(2) Paolesse, R. In *The Porphyrin Handbook*; Kadish, K. M., Smith, K. M., Guilard R., Eds.; Academic Press: San Diego, CA, 2000; Vol. 2, p 201.
(3) Guilard, R.; Barbe, L.-M.; Stem, C.; Kadish, K. M. In *The Porphyrin Handbook*; Kadish, K. M., Smith, K. M., Guilard R., Eds.; Academic Press: Boston, 2003; Vol. 18, p 303.
(4) (a) Ventura, B.; Esposti, A. D.; Koszarna, B.; Gryko, D. T.; Flamigni, L. *New J. Chem.* **2005**, *29*, 1559. (b) Ding, T.; Alemán, E. A.; Modarelli, D. A.; Ziegler, C. J. *J. Phys. Chem. A* **2005**, *109*, 7411.
(5) Gross, Z.; Galili, N.; Saltsman, I. *Angew. Chem., Int. Ed.* **1999**, *38*, 1427.
(6) Paolesse, R.; Jaquinod, L.; Nurco, D. J.; Mini, S.; Sagone, F.; Boschi, T.; Smith, K. M. *Chem. Commun.* **1999**, 1307.

10.1021/ja900220y CCC: $40.75

oligomers have been rather limited in comparison with the extensive lineup of porphyrin counterparts. Kadish et al.[8] reported a series of face-to-face porphyrin−corrole hybrids as well as corrole dimers as promising models of a catalyst for the four-electron reduction of oxygen to water, and Paolesse et al.[9] reported aromatic-bridged corrole dimers and corrole−porphyrin hybrids. Besides these, various corroles have been explored as catalysts,[10] pigments for artificial photosynthesis and solar cells,[11−14] sensors,[15] and so on.[16]

Recent interesting examples include directly linked corrole dimers[17−21] that exhibit unique properties such as strong fluorescence, near-infrared (NIR) transitions, and nonlinear optical (NLO) behavior due to strong electronic interactions, but their fundamental photophysical properties have been far less systematically studied. In this context, we have recently reported the synthesis of singly and doubly β,β'-linked corrole dimers **SH$_3$CD** and **DH$_3$CD** and oxidized forms **DH$_2$CD** and **DZnCD**.[22] This simple set serves as an excellent platform for the examination of detailed intercorrole interactions because of their well-defined geometries. Additionally, we have considered a virtual molecule, oxidized H_2 corrole monomer (**H$_2$CM**), as the constituent corrole unit of **DH$_2$CD**. The molecular structures of these corroles were optimized using density functional theory (DFT) calculations based on X-ray crystallographic structures (Scheme 1).

Scheme 1. Molecular Structures of Corrole Monomers and Dimers Studied in This Work

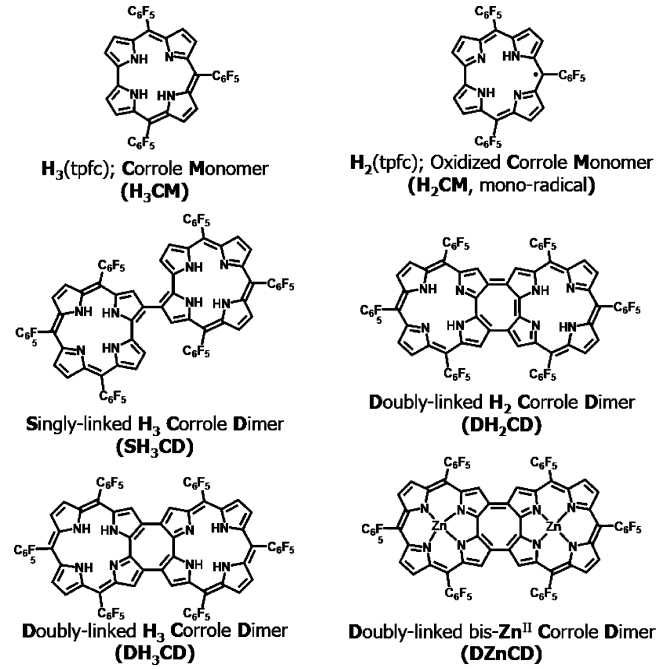

Our work has revealed that an octagonal core in the doubly linked corrole dimers is structurally constrained and subsequently becomes energetically unstable with nonaromatic character. In this regard, the octagonal core acts as an energetic barrier that prohibits electronic communication between the corrole units, so each constituent corrole unit maintains an intrinsic π-conjugation system in spite of the coplanar geometry with a short interchromophoric distance. The unique photophysical properties of the doubly linked corrole dimers, such as intense NIR bands and fast excitation-energy relaxation processes, are attributable to strong molecular orbital (MO) interactions between the corrole units and subsequently perturbed MOs and electronic states. As a consequence, we have been able to reveal the origin of the perturbed electronic structure, the localized aromaticity of the constituent corrole units, and the unusual singlet biradical character of the doubly linked corrole dimers. This work will serve as a firm basis for future studies on elaborated corrole-based functional systems.

II. Experimental Section

Sample Preparation and Steady-State Absorption and Fluorescence Measurements. The directly linked corrole dimers were synthesized by palladium-catalyzed oxidative coupling of 2-borylcorrole using chloroacetone as an oxidant, which afforded the singly β,β'-linked corrole dimer (**SH$_3$CD**).[22] Further oxidation of **SH$_3$CD** with 2,3-dichloro-5,6-dicyano-1,4-benzoquinone (**DDQ**) in toluene provided **DH$_2$CD**. Reduction of **DH$_2$CD** with $NaBH_4$ gave **DH$_3$CD** quantitatively with a concurrent color change from brown to green. In turn, oxidation of **DH$_3$CD** with **DDQ** yielded **DH$_2$CD**, indicating that **DH$_2$CD** is an oxidized form of **DH$_3$CD** and that these two corrole dimers are interconvertible via two-electron redox reactions in a reversible manner.[22] **DH$_2$CD** was metalated with $Zn(OAc)_2 \cdot 2H_2O$ in refluxing $CHCl_3$ to afford **DZnCD**. Dichloromethane solvent was purchased from Sigma-Aldrich (spectrophotometric grade, ≥99.5% purity) and used without further

(7) (a) Gryko, D. T. *Chem. Commun.* **2001**, 2243. (b) Collman, J. P.; Decreau, R. A. *Tetrahedron Lett.* **2003**, *44*, 1207.
(8) Kadish, K. M.; Ou, Z.; Shao, J.; Gros, C. P.; Barbe, J.-M.; Jerome, F.; Bolze, F.; Burdet, F.; Guilard, R. *Inorg. Chem.* **2002**, *41*, 3990.
(9) Paolesse, R.; Pandey, R. K.; Forsyth, T. P.; Jaquinod, L.; Gerzevske, K. R.; Nurco, D. J.; Senge, M. O.; Licoccia, S.; Boschi, T.; Smith, K. M. *J. Am. Chem. Soc.* **1996**, *118*, 3869.
(10) (a) Aviv, I.; Gross, Z. *Chem. Commun.* **2007**, 1987. (b) Gross, Z.; Gray, H. B. *Adv. Synth. Catal.* **2004**, *346*, 165. (c) Yang, H.-Y.; Lai, T.-S.; Yeung, L.-L.; Chang, C. K. *Org. Lett.* **2003**, *5*, 617. (d) Harischandra, D. N.; Zhang, R.; Newcomb, M. *J. Am. Chem. Soc.* **2005**, *127*, 13776.
(11) Tasior, M.; Gryko, D. T.; Cembor, M.; Jawrski, J. S.; Ventura, B.; Flamigni, L. *New. J. Chem.* **2007**, *31*, 247.
(12) Flamigni, L.; Ventura, B.; Tasior, M.; Becherer, T.; Langhals, H.; Gryko, D. T. *Chem.—Eur. J.* **2008**, *14*, 169.
(13) D'Souza, F.; Chitta, R.; Ohkubo, K.; Tasior, M.; Subbaiyan, N.; Zandler, M. E.; Rogacki, M. K.; Gryko, D. T.; Fukuzumi, S. *J. Am. Chem. Soc.* **2008**, *130*, 14263.
(14) Gros, C. P.; Brisach, F.; Meristoudi, A.; Espinosa, E.; Guilard, R.; Harvey, P. D. *Inorg. Chem.* **2007**, *46*, 125.
(15) (a) Barbe, J.-M.; Canard, G.; Brandes, S.; Jerome, F.; Guilard, R. *Dalton Trans.* **2004**, 1208. (b) Barbe, J.-M.; Canard, G.; Brandes, S.; Guilard, R. *Angew. Chem., Int. Ed.* **2005**, *44*, 3103. (c) Barbe, J.-M.; Canad, G.; Brandes, S.; Guilard, R. *Chem.—Eur. J.* **2007**, *13*, 2118.
(16) (a) Adamian, V. A.; D'Souza, F.; Licoccia, S.; Vonas, M. L. D.; Tassoni, E.; Paolesse, R.; Boschi, T.; Kadish, K. M. *Inorg. Chem.* **1995**, *34*, 532. (b) Kadish, K. M.; Adamian, V. A. A.; Caemelbecke, E. V.; Guelectii, E.; Will, S.; Erben, C.; Vogel, E. *J. Am. Chem. Soc.* **1998**, *120*, 11986. (c) Saltsman, I.; Mahammed, A.; Goldberg, I.; Tkachenko, E.; Botoshansky, M.; Gross, Z. *J. Am. Chem. Soc.* **2002**, *124*, 7411. (d) Steene, E.; Dey, A.; Ghosh, A. *J. Am. Chem. Soc.* **2003**, *125*, 16300. (e) Paolesse, R.; Nardis, S.; Stefanelli, M.; Fronczek, F.; Vicente, M. G. H. *Angew. Chem., Int. Ed.* **2005**, *44*, 3047. (f) Gros, C. P.; Barbe, J.-M.; Espinosa, E.; Guilard, R. *Angew. Chem., Int. Ed.* **2006**, *45*, 5642. (g) Hiroto, S.; Hisaki, I.; Shinokubo, H.; Osuka, A. *Angew. Chem., Int. Ed.* **2005**, *44*, 6763. (h) Ruppert, R.; Jeandon, C.; Callot, H. J. *J. Org. Chem.* **2008**, *73*, 694.
(17) Mahammed, A.; Giladi, I.; Goldberg, I.; Gross, Z. *Chem.—Eur. J.* **2001**, *7*, 19.
(18) Luobeznova, I.; Simkhovich, L.; Goldberg, I.; Gross, Z. *Eur. J. Inorg. Chem.* **2004**, 1724.
(19) Sankar, J.; Rath, H.; Prabhuraja, V.; Gokulnath, S.; Chandrashekar, T. K.; Purohit, C. S.; Verma, S. *Chem.—Eur. J.* **2007**, *13*, 105.
(20) Koszarna, B.; Gryko, D. T. *Chem. Commun.* **2007**, 2994.
(21) Barata, J. F. B.; Silva, A. M. G.; Neves, M. G. P. M. S.; Tomé, A. C.; Silva, A. M. S.; Cavaleiro, J. A. S. *Tetrahedron Lett.* **2006**, *47*, 8171.
(22) Hiroto, S.; Furukawa, K.; Shinokubo, H.; Osuka, A. *J. Am. Chem. Soc.* **2006**, *128*, 12380.

purification. UV−vis absorption spectra were recorded with a Cary-5000 UV−vis−NIR spectrometer, and steady-state fluorescence spectra were measured using a Shimadzu RF-2500 fluorometer.

Femtosecond Transient Absorption Experiments. The dual-beam femtosecond time-resolved transient absorption spectrometer consisted of a self-mode-locked femtosecond Ti:sapphire laser (Coherent, MIRA), a Ti:sapphire regenerative amplifier (Clark MXR, CPA-1000) pumped by a Q-switched Nd:YAG laser (ORC-1000), a pulse stretcher/compressor, and an optical detection system.[23,24] The second-harmonic pump beam (400 nm) was focused to a 1 mm diameter spot, and the laser fluence was adjusted to less than ~1.0 mJ cm^{-2} using a variable neutral-density filter. The residual beam was focused onto a flowing water cell to generate a white-light continuum as a probe beam, which was again split into two parts. One part of the white-light continuum was overlapped with the pump beam at the sample to probe the transient, while the other part was passed through the sample without overlapping the pump beam. The time delay between the pump and probe beams was controlled by making the pump beam travel along a variable optical delay. The white-continuum beams after the sample were detected by a fast photodiode. The voltage signals from two photodiodes were sent to a boxcar averager and then processed to calculate the absorption difference spectrum at the desired time delay between the pump and probe pulses.

Nanosecond Time-Resolved Fluorescence Decay Measurements. A time-correlated single-photon counting (TCSPC) system was used for the spontaneous fluorescence decay measurements.[25] The system consisted of a cavity-dumped Kerr lens mode-locked Ti:sapphire laser pumped by a continuous wave Nd:YVO_4 laser (Coherent, Verdi). The second-harmonic of the fundamental beam was generated in a 1 mm thick BBO crystal and served as an excitation source. The residual beam was used as a trigger source detected by a fast photodiode. The excitation beam was focused onto a 10 mm thick cuvette containing the sample solution using a 5 cm focal length lens with s polarization. The fluorescence from the sample was collected and focused onto a monochromator (Acton Research) by a 2″ plano-convex lens pair and detected using a microchannel plate photomultiplier tube (Hamamatsu). The full width at half-maximum (fwhm) of the instrument response function obtained for a dilute solution of coffee cream (diffuser) was typically ~70 ps in our TCSPC system. To obtain the isotropic fluorescence decay profiles, the fluorescence decays were measured at the magic angle (54.7°) using a linear polarizer between the monochromator and the 2″ lens pair. The number of fluorescence photons per unit time was always maintained at <1% of the repetition rate of the excitation pulses to prevent pile-up distortion in the decay profiles.

Two-Photon Absorption Experiments. The two-photon absorption (TPA) spectrum was measured in the NIR region using the open-aperture Z-scan method with 130 fs pulses from an optical parametric amplifier (Light Conversion, TOPAS) operating at a repetition rate of 5 kHz generated from a Ti:sapphire regenerative amplifier system (Spectra-Physics, Hurricane).[26] The NIR beam was divided into two parts. One was monitored by a Ge-PIN photodiode (New Focus) as an intensity reference, and the other was used for the transmittance measurement. After passing through a 10 cm focal length lens, the laser beam was focused and passed through a 1 mm quartz cell. Since the position of the sample cell could be controlled along the laser beam direction (z axis) using the motor-controlled delay stage, the local power density within the sample cell could be simply controlled under constant laser intensity. The transmitted laser beam from the sample cell was then detected by the same photodiode as used for reference monitoring. The on-axis peak intensity of the incident pulses at the focal point, I_0, ranged from 40 to 60 GW cm^{-2}. For a Gaussian beam profile, the nonlinear absorption coefficient β can be obtained by curve fitting of the observed open-aperture traces $T(z)$ with the following equation:

$$T(z) = 1 - \frac{\beta I_0 (1 - e^{-\alpha_0 l})}{2\alpha_0 [1 + (z/z_0)^2]}$$

where α_0 is the linear absorption coefficient, l the sample length, and z_0 the diffraction length of the incident beam.

After the nonlinear absorption coefficient β has been obtained, the TPA cross section $\sigma^{(2)}$ of one solute molecule (in units of GM, where 1 GM = 10^{-50} cm^4 s $photon^{-1}$ $molecule^{-1}$) can be determined by using the following relationship:

$$\beta = \frac{10^{-3} \sigma^{(2)} N_A d}{h\nu}$$

where N_A is the Avogadro constant, d is the concentration of the compound in solution, h is the Planck constant, and ν is the frequency of the incident laser beam.

We obtained TPA spectra of **DH_3CD** at 1300−1500 nm with a 50 nm step as well as those for the oxidized corrole dimers at 2300 nm, where linear absorption is negligible, to satisfy the condition of $\alpha_0 l < 1$ in retrieving the pure TPA $\sigma^{(2)}$ values in the simulation procedure. We also measured a value of 50 GM at 800 nm for the TPA cross section of the reference compound AF-50.

Theoretical Calculations. We calculated the optimized molecular structures and electronic states of a series of corroles using DFT with the (U)B3LYP Hamiltonian and 6-31G* basis set on a supercomputer (KISTI, IBM p690).[27] The initial structures of the corroles except **SH_3CD** and **H_2CM** were based on the X-ray crystal structures. The initial molecular structures of **SH_3CD** and **H_2CM** were obtained from **H_3CM** and **DH_2CD**, respectively; in particular, we examined several initial structures of **SH_3CD** having dihedral angles between corrole units ranging from 0 to 180° to obtain the optimized structure with the lowest total energy. We used the **OPT**, **TD**, and **NMR** keywords to optimize the molecular structures, simulate the electronic states, and obtain theoretical ^{1}H NMR data and nucleus-independent chemical shift (NICS) values,[28] respectively. On the basis of the optimized molecular structures, we calculated harmonic oscillator model of aromaticity (HOMA) values[29] to compare the aromaticities of corrole monomers and constituent corrole units in dimers.

III. Results

Optimized Molecular Structures. While the overall molecular structure of **H_3CM** is similar to that of free-base porphyrin, the planarity of **H_3CM** is not perfect because the smaller cavity size and three inner NH hydrogens induce substantial steric distortions. Therefore, the mean plane deviation (d_{mean}) of constituent atoms in **H_3CM** (excluding the hydrogens and meso substituents) is ~60 times larger than that of free-base porphyrin (0.122 Å in **H_3CM** vs 0.002 Å in tetraphenylporphyrin). In this study, we used the mean plane deviation of **H_3CM** as an important parameter indicating the structural distortion of the corrole units.

The two corrole units in optimized singly linked **SH_3CD** are tilted with respect to each other by a dihedral angle (θ_d) of 58.4°

(23) Ahn, T. K.; Kim, K. S.; Kim, D. Y.; Noh, S. B.; Aratani, N.; Ikeda, C.; Osuka, A.; Kim, D. *J. Am. Chem. Soc.* **2006**, *128*, 1700.
(24) Ahn, T. K.; Kwon, J. H.; Kim, D. Y.; Cho, D. W.; Jeong, D. H.; Kim, S. K.; Suzuki, M.; Shimizu, S.; Osuka, A.; Kim, D. *J. Am. Chem. Soc.* **2005**, *127*, 12856.
(25) Hwang, I.-W.; Cho, H. S.; Jeong, D. H.; Kim, D.; Tsuda, A.; Nakamura, T.; Osuka, A. *J. Phys. Chem. B* **2003**, *107*, 9977.
(26) (a) Kim, D. Y.; Ahn, T. K.; Kwon, J. H.; Kim, D.; Ikeue, T.; Aratani, N.; Osuka, A.; Shigeiwa, M.; Maeda, S. *J. Phys. Chem. A* **2005**, *109*, 2996. (b) Tsuda, A.; Furuta, H.; Osuka, A. *J. Am. Chem. Soc.* **2001**, *123*, 10304.
(27) Cho, S.; Yoon, M.-C.; Kim, C. H.; Aratani, N.; Mori, G.; Joo, T.; Osuka, A.; Kim, D. *J. Phys. Chem. C* **2007**, *111*, 14881.
(28) Chen, Z.; Wannere, C. S.; Corminboeuf, C.; Puchta, R.; Schleyer, P. v. R. *Chem. Rev.* **2005**, *105*, 3842.
(29) Krygowski, T. M.; Cyrański, M. K. *Chem. Rev.* **2001**, *101*, 1385.

Table 1. Information for the Optimized Molecular Structures of Corrole Monomers and Dimers

				NICS (ppm)		HOMA		
	d_{cc} (Å)	θ_d (deg)	d_{mean} (Å)	corrole	oct. core	corrole	oct. core	HOMO−LUMO gap (eV)
H_3CM[a]	−	−	0.122	−12.9	−	0.789	−	2.558
H_3CM[b]			0.165	−12.8	−	0.772		2.543
SH_3CD	8.88	58.4	0.126	−12.7	−	0.777	−	2.438
DH_3CD	8.51	31.8	0.165	−11.5	+8.95	0.772	0.275 0.773	2.101
H_2CM[a]	−	−	0.032	+12.6	−	0.729	−	α: 2.667; β: 1.438
H_2CM[b]			0.024	+28.1	−	0.584	−	α: 2.635; β: 1.194
DH_2CD	8.60	1.22	0.024	+25.5	−4.31	0.584	0.033	0.881
DZnCD	8.66	8.92	0.066	−	−6.56	0.697	−0.001	0.876

[a] Corrole monomer structure optimized using DFT calculations (UB3LYP/6-31G*). [b] Constituent corrole monomer in the optimized doubly linked corrole dimer, without additional optimization.

because of steric hindrance between the corrole units. However, the mean plane deviation in each constituent corrole unit in **SH_3CD** is nearly the same as that in **H_3CM** because of an easy rotation around the single β,β′-linkage (Table 1). On the other hand, doubly linked **DH_3CD** exhibits a ruffled structure with a dihedral angle of 31.8° between the mean planes of the constituent corrole units. Nevertheless, the overall structure of **DH_3CD** is very smooth with a nearly coplanar geometry (see the Supporting Information). It should be noted that two NH hydrogens are found on the side of the direct pyrrole−pyrrole bond in **H_3CM**, while one NH hydrogen is moved to the opposite (distal) side of each corrole in **DH_3CD** (Scheme 1). Since the double β,β′-linkage restricts the freedom of the linked pyrrole rings in the corrole units and also shortens the direct pyrrole−pyrrole bond, the inside NH hydrogen has to move to avoid the increased steric repulsion between neighboring NH hydrogens. Despite this move, the mean plane deviation of the constituent corrole unit in **DH_3CD** increases to 0.165 Å, which clearly shows the structural distortion of the constituent corrole units caused by the double β,β′-linkage. While the center-to-center distance (d_{cc}) between corrole units in **DH_3CD** is slightly smaller than that in **SH_3CD** (8.51 vs 8.88 Å, respectively) because of the coplanar geometry, the lengths of the β,β′-linkages in **SH_3CD** and **DH_3CD** are nearly the same (1.45 and 1.46 Å, respectively). Thus, the electronic conjugation between corrole units in **DH_3CD** is considered to be insignificant despite the coplanar structure.

The oxidized form **DH_2CD** exhibits a nearly flat geometry and a 5 times smaller mean plane deviation of the constituent corrole units (d_{mean} = 0.0241 Å) because of the elimination of one NH hydrogen in each corrole unit and the resultant reduced hydrogen steric repulsion. The bis[zinc(II)] complex **DZnCD** shows a slightly ruffled structure because the corrole cavity is not large enough to accommodate the zinc(II) ion inside the cavity without structural deformation. As a consequence, the mean plane deviation of each corrole unit in **DZnCD** (d_{mean} = 0.0655 Å) is slightly larger than in **DH_2CD** but still 2.5 times smaller than in **DH_3CD**. Importantly, although the interchromophoric distances between the corrole units in **DH_2CD** and **DZnCD** (8.60 and 8.66 Å, respectively) are slightly longer than in **DH_3CD**, the lengths of the β,β′-linkages in **DH_2CD** and **DZnCD** (1.43 and 1.42 Å, respectively) are distinctly reduced. Accordingly, the shorter β,β′-linkages in the oxidized corrole dimers may induce enhanced electronic interactions between the corrole units. Additionally, the overall structure of optimized **H_2CM** is nearly the same as that of the constituent corrole units in **DH_2CD**. However, the mean plane deviation in optimized **H_2CM** (d_{mean} = 0.0318 Å) is slightly larger than that in **DH_2CD**, which also shows the structural restriction of the constituent corrole unit in **DH_2CD**. Thus, it may be concluded that double β,β′-linkage enforces the coplanar geometry with a short interchromophoric distance but also induce structural restrictions on the constituent corrole units as well. The structural information for the optimized corroles is summarized in Table 1.

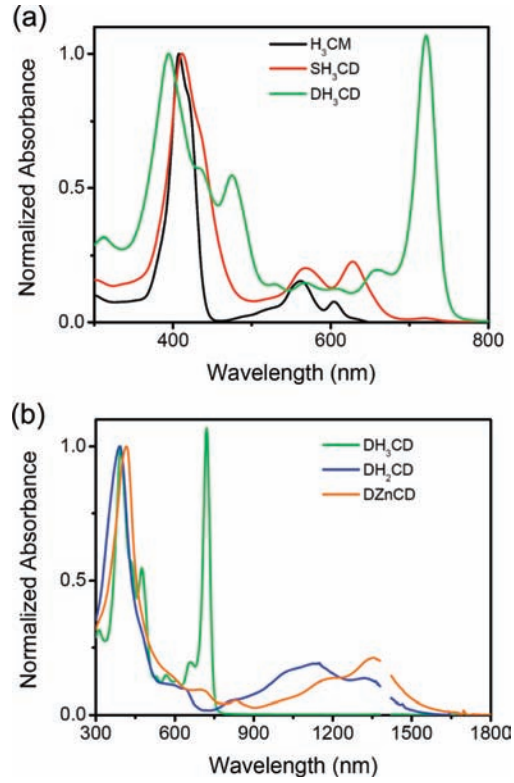

Figure 1. Steady-state absorption spectra of corroles in CH_2Cl_2: (a) corrole **H_3CM** and corrole dimers **SH_3CD** and **DH_3CD**; (b) dimer **DH_3CD** and the oxidized corrole dimers **DH_2CD** and **DZnCD**.

Spectroscopic Properties. Figure 1 shows the steady-state absorption spectra of various corroles. **H_3CM** exhibits a strong B-band at 405 nm and weak Q-bands at 561 and 606 nm. While the overall absorption spectrum of **SH_3CD** does not show a large difference from that of **H_3CM**, the broad B-band with a red-edge shoulder in the **SH_3CD** spectrum implies the existence of various conformers induced by the variation of the dihedral angle between the corrole units and various subsequent *J*-type excitonic interactions in these conformers.[30] Additionally, the red-shifted and enhanced absorption band of **SH_3CD** at 627 nm

(30) Kasha, M.; Rawls, H. H.; El-Bayoumi, M. A. *Pure Appl. Chem.* **1965**, *11*, 371.

Table 2. Photophysical Data for Corrole Monomer and Dimers

	absorption[a]							
	B-band	Q-band	NIR band	fluorescence λ_{max} (nm)	Stokes shift (cm^{-1})	Φ_F[b]	τ_{fluor} (ns)[c]	τ_{bleach} (ps)[c]
H_3CM	405 [95000] 421 [87100]	561 [17600] 606 [8760]	–	615, 642, 661	241	0.13	4.9 (100)	–
SH_3CD	407 [138000] 429 [141000]	568 [40600] 627 [45300]	–	642, 663, 683	372	0.128	2.6 (100)	–
DH_3CD	394 [119000] 438 [59200] 477 [61800]	525 [16300] 571 [17200] 662 [23300] 722 [123000]	–	737, 800	283	0.032	0.2 (65.4) 2.2 (34.6)	–
DH_2CD	390 [110000] 469 [29900]	565 [9580] 632 [9820]	1053 [16200] 1157 [12100] 1320 [15000]	–	–	–	–	7.4 (100)
DZnCD	411 [89000] 442 [49900]	514 [17800] 599 [13600] 701 [11500] 715 [9130]	1110 [9700] 1345 [24700]	–	–	–	–	7.2 (100)

[a] λ_{max} (nm) [ε (M^{-1} cm^{-1})]. [b] Fluorescence quantum yield [reference: **H_3CM** in CH_2Cl_2 (Φ_F = 0.13)]. [c] Values in parentheses are percentages of the total amplitude.

is a clear indication of perturbed configurational interactions in the S_1 state as a result of MO interactions. However, the electronic perturbation in **SH_3CD** is not so significant because of the largely tilted geometry.

It should be noted that the **DH_3CD** absorption spectrum is largely different from those of **H_3CM** and **SH_3CD**, as it includes broad, split B-bands and a newly generated strong absorption band at 722 nm, whose intensity (ε_{722nm} = 128 000 M^{-1} cm^{-1}) is comparable to that of the B-band (ε_{396nm} = 120 000 M^{-1} cm^{-1}). Since the coplanar structure of **DH_3CD** induces *H*- and *J*-type excitonic interactions simultaneously, the split B-bands can be explained in terms of an excitonic coupling model.[32] However, the newly generated strong absorption band at 722 nm with a narrow bandwidth (~530 cm^{-1}) cannot be explained by the exciton coupling. This will be discussed later.

The fluorescence spectra of **H_3CM**, **SH_3CD**, and **DH_3CD** exhibit mirror images of the absorption spectra with small Stokes shifts in the range 250−350 cm^{-1} (Table 2). Compared with **H_3CM** and **DH_3CD**, **SH_3CD** exhibits slightly broader and more featureless fluorescence spectra, presumably because of the distribution of dihedral angles between corrole units along the single β,β'-linkage. The temporal fluorescence profiles of **H_3CM** and **SH_3CD** exhibit single-exponential decay with the time constants (τ_{fluor}) of 4.87 and 2.63 ns, respectively. In contrast, **DH_3CD** exhibits double-exponential decay with time constants of 0.21 and 2.15 ns (Table 2; also see the Supporting Information). On the basis of the fluorescence quantum yields and the average fluorescence lifetimes, we found that the radiative and nonradiative decay rates in **DH_3CD** are nearly the same as and 6 times faster, respectively, than those of **H_3CM** (see the Supporting Information). Accordingly, the fast fluorescence decay component of **DH_3CD** seems to be correlated with the existence of a hypothetical nonradiative electronic state below the dipole-allowed S_1 state.

The oxidized corrole dimers, **DH_2CD** and **DZnCD**, exhibit broad NIR absorption bands without any fluorescence (Figure 1b). Since the absorption spectra of the oxidized corrole dimers in CH_2Cl_2 and toluene are nearly the same and the band width of the NIR band of **DH_2CD** is only 2 times that of Q-band of **H_3CM** (1200 and 540 cm^{-1}, respectively), we expect that the NIR bands of the oxidized corrole dimers probably arise from

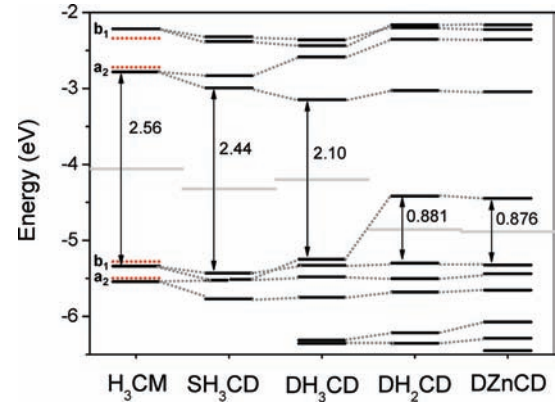

Figure 2. MO energy diagram of corrole monomer and dimers based on the optimized molecular structures. The red dotted lines in **H_3CM** indicate MO levels of the structurally constrained **H_3CM** unit in **DH_3CD**.

singlet excited states and not from charge-transfer (CT) or n → π^* transitions. In this regard, the largely red-shifted absorption bands of the oxidized corrole dimers without large structural changes or additional substituents are very unique.

The temporal bleaching signals of **DH_2CD** and **DZnCD** show fast recovery processes with time constants (τ_{bleach}) of 7.4 and 7.2 ps, respectively (see the Supporting Information). Accordingly, the abruptly shortened excited-state lifetimes of **DH_2CD** and **DZnCD** well support nonfluorescent behaviors, providing evidence for the new lower-lying electronic states in the NIR region that probably play an important role in the excitation-energy relaxation processes. The photophysical data based on the steady-state and time-resolved experiments are summarized in Table 2.

Molecular Orbitals and Electronic Structures. We simulated the electronic states on the basis of the optimized molecular structures in order to reveal the origin of the newly generated electronic states of the doubly linked corrole dimers. Since the β,β'-linkages of the corrole dimers give rise to a short interchromophoric distance of 8.5−8.9 Å between the corrole units, the MOs of the corrole units are mixed and split depending on the relative orientation of the corrole units as well as on the MO shapes (Figure 2). Basically, the B- and Q-states of **H_3CM** (C_{2v}) are generated by the configurational interactions of four frontier MOs: two HOMO-like MOs [HOMO (b_1) and HOMO−1 (a_2)] and two LUMO-like MOs [LUMO (a_2) and

(31) Gouterman, M. In *The Porphyrins*; Dolphin, D., Ed.; Academic Press: New York, 1978; Vol. III, Part A: Physcal Chemistry.

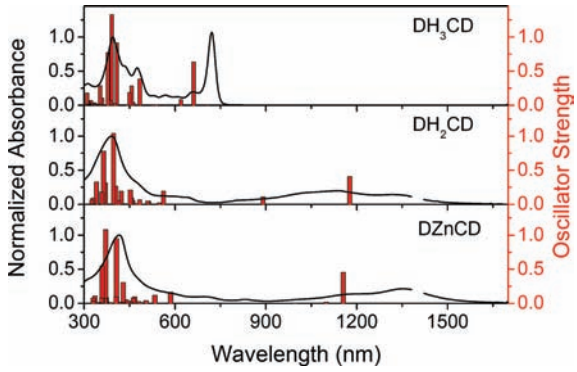

Figure 3. Simulated electronic states of **DH$_3$CD**, **DH$_2$CD**, and **DZnCD** obtained using time-dependent DFT calculations with the B3LYP Hamiltonian (nstate = 40). Since the simulation of the electronic states was done without consideration of solvation effects, the simulated electronic states are in a higher-energy region than the absorption spectra.

LUMO+1 (b_1)], which have been used in Gouterman's four-orbital model for tetrapyrrolic macrocycles.[31,32] In the β,β'-linked corrole dimers, the a_2-symmetric MOs strongly interact with each other, and the MO level is split by a larger amount than for the b_1-symmetric MOs because the a_2-symmetric MOs of the corrole unit, HOMO−1 and LUMO, exhibit large electronic densities on the linking β-carbons. As a result, the MO degeneracy is broken, and the configurational interactions in the corrole dimers become complicated (Figure 2). While **SH$_3$CD** has one β,β'-linkage and therefore exhibits a largely tilted geometry, **DH$_3$CD** takes the coplanar geometry supported by the double β,β'-linkage, and consequently, stronger MO interactions between corrole units occur in **DH$_3$CD**, resulting in distinctly split MOs and a smaller HOMO−LUMO gap (2.10 eV) than in **SH$_3$CD** (2.44 eV). The simulated electronic states of the corroles are well-matched with the steady-state absorption spectra (Figure 3). On the basis of these simulated electronic states, we can reveal the origin of the newly generated strong absorption band at 722 nm of **DH$_3$CD** as arising from the optically allowed HOMO−LUMO transition. Since the stabilized LUMO and destabilized HOMO in **DH$_3$CD** are evident, Gouterman's four-orbital model is not applicable (Figure 2). In addition, it is particularly noteworthy that the lowest forbidden singlet excited state is located below the optically allowed singlet state (see the Supporting Information). The observed fast decay component in the temporal S_1 fluorescence profile and the accelerated nonradiative rate of the S_1 state of **DH$_3$CD** are probably correlated with this lowest forbidden state. Although **DH$_3$CD** exhibits a rigid structure and an optically allowed transition in the Q-band region, the fluorescence quantum yield of **DH$_3$CD** is 4 times smaller than that of **H$_3$CM** or **SH$_3$CD** (Table 2).

In the oxidized corrole dimers **DH$_2$CD** and **DZnCD**, the electrochemical HOMO−LUMO energy gaps were determined to be dramatically reduced to less than 0.9 eV (Table 1). On the basis of the comparative MO analysis, we found that the origins of the LUMOs of the oxidized dimers and the HOMO of **DH$_3$CD** are the same (see the Supporting Information). The conversion from HOMO to LUMO in the oxidized dimers could be achieved by the rigid backbone of corrole and an elimination of two π electrons by the oxidation reaction. Since the shorter β,β'-linkages of the oxidized corrole dimers relative to those of **DH$_3$CD** induce stronger MO interactions between the corrole units and a larger MO splitting (Figure 2), many new electronic states of **DH$_2$CD** and **DZnCD** appear in the NIR region (Figure 3). Remarkably, the lowest singlet excited states of **DH$_2$CD** and **DZnCD** are located at 0.43 and 0.34 eV, respectively, and arise from HOMO−LUMO transitions, which are well-matched with the gap between the first oxidation and reduction potentials (0.40 V for **DZnCD**).[24] However, these lowest singlet states are not shown in the steady-state absorption spectra because of their small oscillator strengths. Since the MO symmetries of the HOMO and LUMO of the oxidized corrole dimers (D_{2h}) are assigned as B_{2g} and A_u, respectively, the HOMO−LUMO transition has B_{2u} symmetry (y-polarized, short molecular axis), which is optically allowed but energetically forbidden. On the other hand, since the HOMO−2 has B_{3g} symmetry, the HOMO−2-to-LUMO transition has B_{3u} symmetry (x-polarized, long molecular axis) and becomes optically allowed, producing the intense NIR absorption bands at 1300 nm in the steady-state absorption spectra (see the Supporting Information). Although the lower-lying electronic states of **DH$_2$CD** and **DZnCD** are optically forbidden, these lowest excited states presumably provide nonradiative decay pathways in the excitation-energy relaxation processes by acting as a deactivation ladder between the excited and ground states.

IV. Discussion

Aromaticity of Corroles. H$_3$CM is a representative aromatic molecule with an 18-π macrocyclic conjugation pathway.[33] Since the nonplanar structure of corrole is easily perturbed by an external stimulus, corrole can be a good test bed for exploring the relationship between aromaticity and molecular structure. Generally, the π-electron delocalization of cyclic aromatic molecules results in electronic stabilization, small bond-length alternation (BLA), and generation of a diatropic ring current. On the contrary, antiaromatic molecules exhibit electronic destabilization, a localized π-electron distribution, and a paratropic ring current.[34] To quantify the aromaticity of the corroles, we calculated NICS[28] and HOMA[29] values. The NICS calculation is a computational method that calculates the chemical shift of a hypothetical lithium ion positioned directly inside the ring [a value in parentheses is the distance (in Å) from the mean plane].[28] In this method, the negative and positive signs of the NICS values represent aromaticity and antiaromaticity, respectively, and the amplitudes of the NICS values can be used as a quantitative measure of aromaticity. On the other hand, the HOMA value is defined as a normalized sum of squared deviations of bond lengths from the optimal value, which is assumed to be realized for a fully aromatic molecular system. Accordingly, HOMA could be used as a structural definition of aromaticity, and the proper equation for HOMA is

$$\mathrm{HOMA} = 1 - \frac{\alpha}{n}\sum_i (R_{\mathrm{opt}} - R_i)^2$$

$$= 1 - \left[\alpha(R_{\mathrm{opt}} - R_{\mathrm{av}})^2 + \frac{\alpha}{n}\sum_i (R_{\mathrm{av}} - R_i)^2\right] = 1 - [\mathrm{EN} + \mathrm{GEO}] \quad (1)$$

where n is the number of bonds taken into the summation, α is an empirical constant chosen to give HOMA = 0 for the hypothetical Kekulé structures of aromatic systems and 1 for

(32) Gouterman, M. *J. Mol. Spectrosc.* **1961**, *6*, 138.

(33) (a) Aihra, J.-I. *J. Phys. Chem. A* **2008**, *112*, 5305. (b) Johnson, A. W.; Kay, I. T. *J. Chem. Soc.* **1965**, 1620.

(34) Schleyer, P. v. R. *Chem. Rev.* **2001**, *101*, 1115.

Scheme 2. Diatropic Ring Current in **H_3CM** and Strong Paramagnetism Outside the Direct Pyrrole−Pyrrole Bond

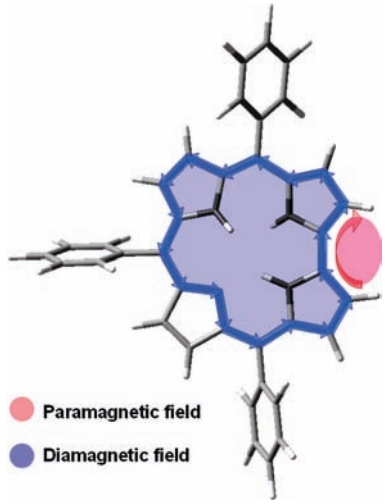

the system with all bonds equal to the optimal value R_{opt}, and R_{av} is the average bond length.[29] While the HOMA values of aromatic molecules are close to 1, those of nonaromatic molecules are nearly zero.

We first calculated the NICS and HOMA values of aromatic **H_3CM** as a reference. **H_3CM** has a negative NICS(0) value of −12.9 ppm and a large HOMA value of 0.789, indicating the aromaticity of **H_3CM**. Interestingly, on the basis of the transverse NICS scan of **H_3CM** along the molecular axis, we found that the rim outside the direct pyrrole−pyrrole bond exhibits 2−3 times larger positive NICS(0) values than the other outer rim of corrole (see the Supporting Information). We carried out the comparative NICS calculations of sapphyrin (aromatic) and isosmaragdrin (aromatic) with similar local structures, which confirmed that the direct pyrrole−pyrrole bond of an aromatic molecule induces a relatively strong paramagnetic region at the outside, presumably because this area is surrounded by three covalent bonds, and additionally that the reverse torque of the diatropic ring current shown in Scheme 2 could be responsible for the induced paramagnetic field. In **SH_3CD**, the NICS(0) and HOMA values of each constituent corrole unit (−12.7 ppm and 0.777, respectively) are similar to those of **H_3CM**, indicating that the intrinsic aromaticity of corrole is maintained in **SH_3CD** and that the single β,β'-linkage does not perturb the aromaticity and resonance structure of the constituent corrole units.

The NICS(0) and HOMA values of the constituent corrole units in **DH_3CD** were calculated to be −11.5 ppm and 0.772, respectively, which are similar to those of **H_3CM** and **SH_3CD**, indicating that the intrinsic aromaticity of the corrole units is also maintained in spite of the structural distortion and relocation of the NH hydrogen. On the other hand, the octagonal core in **DH_3CD** exhibits a positive NICS(0) value of +8.95 ppm, with a large out-of-plane NICS(0) value of +40.6 ppm and a vertical NICS scan spectrum typical of antiaromatic molecules, showing an obvious antiaromatic sign (see the Supporting Information). To reveal the origin of the paramagnetism at the octagonal core, we carried out transverse NICS calculations for **DH_3CD**. As a result, we found that the transverse NICS scan spectrum of **DH_3CD** could be expressed as a linear summation of those of the two constituent corrole units (Figure 4), indicating that the paramagnetism at the octagonal core in **DH_3CD** is caused by the overlap of the induced paramagnetic region outside the direct

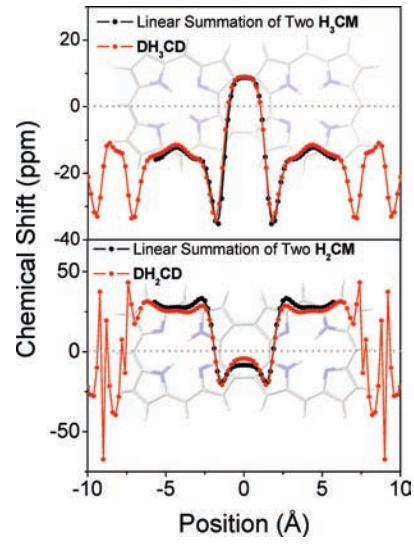

Figure 4. Comparisons of the transverse NICS scan spectra of **H_3CM** and **DH_3CD** and of **H_2CM** and **DH_2CD**.

Scheme 3. Isolated Induced Ring Current in the Doubly Linked Corrole Dimers (Blue and Red Colors Indicate Diamagnetism and Paramagnetism, Respectively)

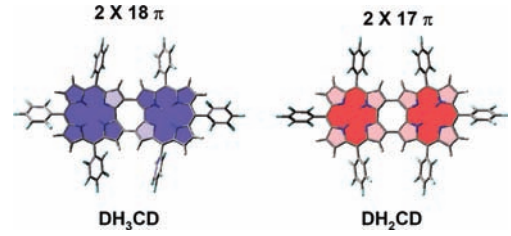

pyrrole−pyrrole bonds of the constituent corrole units. Consequently, we could propose a scheme involving isolated diatropic ring currents in the two corrole units (Scheme 3), and thus, **DH_3CD** could be expressed as a combination of two isolated aromatic corrole units. In contrast, the NICS(0) and HOMA values of the constituent oxidized corrole units in **DH_2CD** were evaluated to be +25.5 ppm and 0.584, respectively. The large positive NICS value as well as the reduced HOMA value of the corrole units in **DH_2CD** is likely in line with its antiaromatic character. At the same time, the octagonal core of **DH_2CD** exhibits the negative NICS(0) value of −4.31 ppm. Prior to further discussion of **DH_2CD**, the virtual **H_2CM** molecule has to be dealt with as a constituent unit in **DH_2CD**. Optimized **H_2CM** is a molecule with a single radical that may be categorized as an antiaromatic because of its large positive NICS(0) value of +12.6 ppm and the typical antiaromatic vertical NICS scan spectrum (see the Supporting Information). However, the NICS(0) value of optimized **H_2CM** is 2 times smaller than that of the constituent oxidized corrole unit in **DH_2CD**. To check the effect of structural variations, we calculated the NICS(0) value of the restricted oxidized corrole monomer extracted from **DH_2CD** without further optimization and obtained the large positive value of +28.1 ppm; also, the transverse NICS spectrum of **DH_2CD** could be also expressed as a linear summation of those of the two restricted constituent oxidized corrole units (Figure 4 and the Supporting Information). Accordingly, the constituent corrole units in **DH_2CD** also seem to maintain their intrinsic antiaromaticity. Additionally, it should be noted that the stronger paramagnetism and reduced HOMA value of the restricted **H_2CM** in **DH_2CD** reflects the enhanced

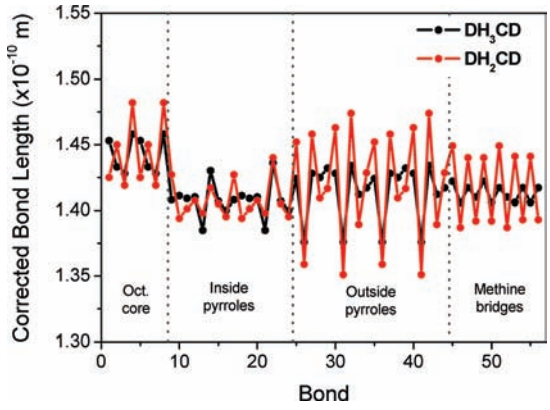

Figure 5. Bond length distributions for **DH$_3$CD** and **DH$_2$CD**.

antiaromatic character caused by the structural restriction imposed by the double β,β'-linkage.

To explain the conservation of the intrinsic aromatic or antiaromatic property of the constituent corrole unit in the doubly linked corrole dimers, we considered the function of the octagonal core. Figure 5 shows the bond length distributions for **DH$_3$CD** and **DH$_2$CD**. The C−N bonds [$R(n)$] were converted into virtual C−C bonds [$r(n)$] via the following formula:[29]

$$r(n) = 1.467 - 0.1702 \ln(m) \quad (2)$$

where

$$m = \exp\left(\frac{1.467 - R(n)}{0.2828}\right)$$

The average bond lengths in the octagonal cores of **DH$_3$CD** and **DH$_2$CD** are 1.443 and 1.444 Å, respectively, which are distinctly longer than those in the other parts of these molecules and far from the optimum values for aromatic systems. The HOMA values of the octagonal cores in **DH$_3$CD** and **DH$_2$CD** are very close to zero (0.179 and 0.033, respectively), and the energetic terms (EN in eq 1) are close to 1 (0.780 and 0.808, respectively), indicating an energetically unfavorable structure and nonaromatic character. Furthermore, while **DH$_2$CD** exhibits large BLA at the outside pyrroles and methine bridges because of its antiaromaticity, the BLA of the octagonal core and inside pyrroles in **DH$_2$CD** is not distinct (Figure 5). Thus, we suggest that the central part of the dimer, including the octagonal core and the four inside pyrroles, is strongly constrained by the double β,β'-linkage, and as a consequence, the energetically unfavorable octagonal core in the doubly linked corrole dimers cannot take a part in π-electron conjugation between the corrole units. Thus, the role of the octagonal core is presumably to serve as an energetic barrier against electronic communication, resulting in the electronic isolation of the two corroles, irrespective of their intrinsic character as either aromatic or antiaromatic species.

Singlet Biradical Character and NLO Properties. In the previous study,[22] it was found on the basis of electron spin resonance (ESR) and temperature-dependent SQUID magnetic susceptibility measurements that **DZnCD** has a stable biradical character with a singlet ground-state. However, the origin of the singlet biradical character has remained uncertain. To reveal the origin of the singlet biradical character of the oxidized corrole dimers, we considered the constituent oxidized corrole monomers. Since the oxidized corrole dimers consist of two oxidized corrole monomers, each with a single radical, the dimers have two unpaired electrons. We therefore suggest that the singlet biradical character of the oxidized corrole dimers originates from the nonbonding character of these two unpaired electrons and their appropriate interactions.[35] As mentioned above, electronic communication between the corrole units is prohibited by the nonaromatic octagonal core, so the intrinsic antiaromaticity as well as the nonbonding property of the oxidized corrole monomer seems to be maintained. At first, to investigate the singlet biradical character of the oxidized corrole dimers, we had to quantify the interaction between the two unpaired electrons. Unfortunately, however, this is very difficult. Therefore, we used an indirect method based on energetic considerations: the theoretical calculation of the energy difference between the lowest singlet and triplet states (ΔE_{S-T}). If the interaction between two unpaired electrons is very weak or nearly zero, the ground state becomes a triplet because of Hund's rule. On the other hand, as the interaction becomes stronger, one orbital exhibits bonding character and the other antibonding character. Consequently, the stabilized bonding orbital gradually becomes doubly occupied, and the spin state changes from triplet to singlet, at which point the open-shell biradical character disappears.

Despite the similar molecular structures, the ΔE_{S-T} values of **DH$_2$CD** and **DZnCD** (0.150 and 0.190 eV, respectively) were calculated to be nearly 10 times smaller than that of **DH$_3$CD** (1.51 eV), reflecting the fact that **DH$_2$CD** and **DZnCD** are energetically far from closed-shell systems. Additionally, the spin state of the doubly linked corrole dimers also had to be considered in order to examine the biradical character. We used the spin-unrestricted (U)B3LYP Hamiltonian and the broken $\alpha-\beta$ and spatial symmetries of the HOMO and LUMO to consider their biradical character. We found that **DH$_3$CD** exhibits a nearly zero spin value of 6.31×10^{-4} while the spin values of **DH$_2$CD** and **DZnCD** are significantly larger (5.73×10^{-1} and 1.39×10^{-2}, respectively), although the oxidized corrole dimers have singlet spin character. Notably, while the ΔE_{S-T} values of **DH$_2$CD** and **DZnCD** are very close, **DZnCD** exhibits a smaller spin value, indicating that the interaction between the two unpaired electrons in **DZnCD** is probably stronger than that in **DH$_2$CD**. In conclusion, we suggest that the oxidized corrole dimers are evidently located in the open-shell singlet biradical region and that the interaction between the two unpaired electrons is appropriate to maintain the nonbonding character of these electrons, which is presumably realized by the prohibition of electronic communication between the corrole units through the octagonal core despite the coplanar geometry and short interchromophoric distance. In addition, **DZnCD** has a more obvious singlet biradical character than **DH$_2$CD** on the basis of the theoretical calculations.

Generally, the neutral orbital occupation number (NOON) of the LUMO is an important parameter in quantifying the extent of radical character. However, in the oxidized corrole dimers, the bonding and antibonding SOMOs become HOMO−1 and HOMO, not HOMO and LUMO, because the MO interactions between the doubly occupied MOs of the constituent corrole units are very strong compared with those of the SOMOs. Thus, the NOON value of the oxidized corrole dimers is too complicated and cannot be directly used to evaluate the radical character. Thus, the ΔE_{S-T} and spin values are more important parameters for estimating the biradical character of the oxidized corrole dimers.

A loosely bound singlet biradical could enhance a third-order NLO response and consequently a TPA activity, which is affected by the partial breaking of the π bond, allowing for an easy distortion

(35) Salem, L.; Rowland, C. *Angew. Chem., Int. Ed.* **1972**, *11*, 92.

Table 3. Energy Differences between Singlet and Triplet States, Spin Values, Calculated Static γ Values, and TPA Cross Sections for the Doubly Linked Corrole Dimers

				TPA data		
	ΔE_{S-T} (eV)	spin	γ_{xxxx} (10^3 au)	excitation wavelength (nm)	concentration (M)	$\sigma^{(2)}$ (GM)
DH_3CD	1.512	6.305×10^{-4}	2100	1400	0.26	1100
DH_2CD	0.1384	5.731×10^{-1}	4540	2100	0.13	3700
DZnCD	0.1900	1.392×10^{-2}	9217	2100	0.16	4600

of the π-electron distribution along the π-conjugated pathway.[36−38] To explore the NLO properties of the oxidized corrole dimers with a focus on the effect of the singlet biradical character, we employed the finite-field approach to calculate the dominant longitudinal component of static γ (γ_{xxxx}) value of the oxidized corrole dimers.[37,38] As a result, the γ values calculated for **DH_2CD** and **DZnCD** are distinctly enhanced (4.540×10^6 and 9.217×10^6 au, respectively) compared with that for **DH_3CD** (2.100×10^6 au). Since **DZnCD** has stronger singlet biradical character as well as the two electron-rich central metals, the largest γ value is achieved for **DZnCD**.

The maximum TPA cross section of closed-shell **DH_3CD** at 720 nm was measured to be $\sigma^{(2)} = 1100$ GM, which is ~22 times larger than that of the corrole monomer at the Q-band (<50 GM).[39] The TPA enhancement in **DH_3CD** is presumably due to the strong MO interactions and subsequently enhanced transition dipole moment. However, the TPA cross section of **DH_3CD** is still 10 times smaller than that of the triply linked free-base porphyrin dimer (13 000 GM).[26] Despite the similar molecular structures and the similar number of π electrons, the large difference between the TPA cross section values of **DH_3CD** and the triply linked porphyrin dimer is likely to be caused by the interrupted electronic communication between the corrole units and the resulting localized electronic structures of the individual corrole units without any distinct CT character.

On the other hand, **DH_2CD** and **DZnCD** exhibit TPA cross sections of 3700 and 4600 GM, respectively, which are enhanced compared with that for **DH_3CD**. Since we did not scan the TPA spectra of the oxidized corrole dimers because of experimental limitations, especially the maximum TPA cross section of **DZnCD** is obviously larger than the measured TPA value at 2100 nm. Nevertheless, the larger TPA values for the oxidized corrole dimers are well-matched with the calculated static γ values and also seem to mainly arise from the singlet biradical character and the additional effect of the central metal. However, the TPA cross sections of the oxidized corrole dimers are still much smaller than that of the triply linked porphyrin dimer. Thus, although the oxidized corrole dimers with singlet biradical character exhibit enhanced TPA cross section and static γ values, the prohibition of electronic communication between the corrole units and the antiaromaticity of the constituent oxidized corrole units negatively affects the TPA activities of the oxidized corrole dimers, leading to the relatively small TPA cross sections relative to those of triply linked porphyrin dimers. The calculated static γ and TPA cross section values of the corrole dimers are summarized in Table 3.

V. Conclusions

We have systematically investigated the structural and photophysical properties of a series of directly linked corrole dimers. The octagonal cores in the doubly linked corrole dimers are structurally constrained, thus serving as an energetic barrier against electric communication between the two corrole units. The resulting unique interchromophoric interactions, prohibited electronic communication, and strong MO interactions between the constituent corrole units in the doubly linked corrole dimers give rise to unusual photophysical properties such as intense NIR absorption bands and singlet biradical character. Especially, the singlet biradical character of the oxidized corrole dimers is induced by two inherent unpaired electrons (one in each of the oxidized corrole monomers) and their appropriate interactions, which could also be realized by the prohibition of electronic communication through the octagonal core. Importantly, these stable biradical species exhibit enhanced NLO properties and large two-photon absorption cross sections. In this work, we have demonstrated that the structural constraints and resulting unique interchromophoric interactions between corrole units play a major role in the overall photophysical properties of the doubly linked corrole dimers.

Acknowledgment. This research was financially supported by the Star Faculty and World Class University (2008-1955) Programs of the Ministry of Education, Science, and Technology of Korea and an AFSOR/AOARD Grant (FA4869-08-1-4097). The quantum-chemical calculations were performed using the supercomputing resources of the Korea Institute of Science and Technology Information (KISTI). The work at Kyoto University was supported by Grants-in-Aid for Scientific Research (19205006, 18655013, and 20108001 "pi-Space") from MEXT. S.C., J.M.L., and P.K. acknowledge fellowships from the BK21 program of MEST. S.H. acknowledges the Research Fellowship for Young Scientists from JSPS. H.S. acknowledges financial support from the Mitsubishi Chemical Corporation Fund.

Supporting Information Available: Macrocyclic conjugation pathway of **H_3CM**, 3D molecular structures of corrole dimers, absorption spectra of various corroles in MC, absorption spectra of **DH_2CD** and **DZnCD** in MC and toluene, simulated electronic states of **H_3CM** and **SH_3CD**, MO energy levels and shapes for the doubly linked corrole dimers, steady-state fluorescence spectra and time-resolved fluorescence decay profiles of corroles, time-resolved bleaching recovery profiles for the oxidized corrole dimers, vertical NICS scan spectra of the constituent corrole units and octagonal cores of **DH_3CD** and **DH_2CD**, vertical NICS scan spectra of optimized **H_2CM** and restricted **H_2CM** from **DH_2CD**, transverse NICS scan spectrum of **H_3CM**, TPA cross section scan spectrum of **DH_3CD**, difference between the BLAs in **DH_3CD** and **DH_2CD**, transition symmetries of D_{2h} **DH_2CD**, simulated electronic states of **H_3CM**, **DH_3CD**, **DH_2CD**, and **DZnCD**, complete ref 36, and CIF files for **DH_2CD**, **DH_3CD**, and **DZnCD**. This material is available free of charge via the Internet at http://pubs.acs.org.

JA900220Y

(36) Ohta, S.; et al. *J. Phys. Chem. A* **2007**, *111*, 3633.
(37) Kamada, K.; Ohta, K.; Kubo, T.; Shimizu, A.; Morita, Y.; Nakasuji, K.; Kishi, R.; Ohta, S.; Furukawa, S.-I.; Takahashi, H.; Nakano, M. *Angew. Chem., Int. Ed.* **2007**, *46*, 3544.
(38) Nakano, M.; Kubo, T.; Kamada, K.; Ohta, K.; Kishi, R.; Ohta, S.; Nakagawa, N.; Takahashi, H.; Furukawa, S.-I.; Morita, Y.; Nakasuji, K.; Yamaguchi, K. *Chem. Phys. Lett.* **2006**, *418*, 142.
(39) Rebane, A.; Drobizhev, M.; Makarov, N. S.; Koszarna, B.; Tasior, M.; Gryko, D. T. *Chem. Phys. Lett.* **2008**, *462*, 246.